

Suppression of spin bath dynamics for improved coherence of multi-spin-qubit systems

N. Bar-Gill,^{1,2} L. M. Pham,³ C. Belthangady,¹ D. Le Sage,¹ P. Cappellaro,⁴ J. R. Maze,⁵ M. D. Lukin,² A. Yacoby,² and R. Walsworth^{1,2}

¹*Harvard-Smithsonian Center for Astrophysics, Cambridge, MA 02138, USA*

²*Department of Physics, Harvard University, Cambridge MA, USA*

³*School of Engineering and Applied Sciences,
Harvard University, Cambridge, MA 02138, USA*

⁴*Department of Nuclear Science and Engineering, MIT, Cambridge MA, USA*

⁵*Department of Physics, Pontificia Universidad Catolica de Chile, Santiago 7820436, Chile*

Scalability of multi-qubit systems is crucial for the advancement and application of quantum science. Such scalability requires maintaining long coherence times while increasing the number of qubits in the system. For solid-state spin systems, qubit coherence is closely related to fundamental questions of many-body spin dynamics. Here we apply a coherent spectroscopic technique to characterize the dynamics of the composite solid-state spin environment of Nitrogen-Vacancy (NV) color centers in room temperature diamond. We identify a new mechanism for suppression of electronic spin bath dynamics in the presence of a nuclear spin bath of sufficient concentration. This suppression enhances the efficacy of dynamical decoupling techniques, resulting in increased coherence times for multi-spin-qubit systems, thus paving the way for scalable applications in quantum information, sensing and metrology.

Understanding and controlling the coherence of multi-spin-qubit solid-state systems is crucial for quantum information science [1–3], basic research on quantum many-body dynamics [4] and quantum sensing and metrology [5–9]. Examples of such systems include Nitrogen-Vacancy (NV) color centers in diamond [10], phosphorous donors in silicon [11] and quantum dots [12]. The relevant Figure-of-Merit (FOM) for scalable multi-qubit systems is the product of the qubit density (n_{qb}) and their coherence lifetime (T_2), $FOM = n_{qb}T_2$. For quantum measurements, the phase-shift sensitivity $\delta\phi$ scales as $1/\sqrt{FOM}$ [5, 13–15]. Increasing this multi-qubit FOM requires an understanding of the sources of decoherence in the system, and their interplay with qubit density. In particular, for solid state spin qubits T_2 is typically limited by interaction with an environment (i.e., bath) of paramagnetic spin impurities; whereas n_{qb} is limited by fabrication issues, the associated creation of additional spin impurities in the environment, and the ability to polarize (state prepare) the quantum spins.

The paradigm of a central spin coupled to a spin environment has been studied intensively for many years (see e.g., [16, 17]); and quantum control methods have been developed to extend the spin coherence lifetime by reducing the effective interaction with the environment. In particular, dynamical decoupling techniques pioneered in NMR have recently been applied successfully to extend the effective T_2 of single NV-diamond electronic spins by more than an order of magnitude [18, 19].

Here we study experimentally the multi-spin-qubit FOM of NV color centers in room temperature diamond (Fig. 1(a,b)). We apply a spectral decomposition technique [20–22] to characterize the dynamics of the composite solid-state spin bath that limits the NV electronic spin T_2 , consisting of both electronic spin (N) and nuclear spin (^{13}C) impurities. We study three different diamond samples with a wide range of NV densities and impurity spin concentrations (see Table 1); and find unexpectedly long correlation times for the electronic spin baths in two diamond samples with natural abundance of ^{13}C nuclear spin impurities. We identify a new mechanism involving an interplay between the electronic and nuclear spin baths that can explain the observed suppression of electronic spin bath dynamics. We show that this spin-bath suppression enhances the efficacy of dynamical decoupling techniques, enabling very large values for the multi-qubit

FOM $\sim 2 \times 10^{14}$ [ms/cm³], which is the largest achieved so far in a room temperature solid-state system (compare, e.g., to [23]). In future work this spin-bath suppression could be used to engineer NV-diamond samples with an even larger multi-spin-qubit FOM, exceeding the current state-of-the-art in any system.

Due to coupling of the NV spins to their magnetic environment, coherence is lost over time with the general form $C(t) = e^{-\chi(t)}$, where the functional $\chi(t)$ describes the time dependence of the decoherence process (Supplement). In the presence of a modulation acting on the NV spins (e.g., a resonant RF pulse sequence), described by a filter function in the frequency domain $F_t(\omega)$ (see below), the decoherence functional is given by [24, 25]

$$\chi(t) = \frac{1}{\pi} \int_0^\infty d\omega S(\omega) \frac{F_t(\omega)}{\omega^2}, \quad (1)$$

where $S(\omega)$ is the spectral function describing the coupling of the system to the environment. Eq. (1) holds in the approximation of weak coupling of the NV spins to the environment, which is appropriate for the (dominantly) electronic spin baths of the diamond samples discussed here [17] (see below).

The spectral decomposition technique allows us to determine $S(\omega)$ from straightforward decoherence measurements of the NV spin qubits. As seen from Eq. (1), if an appropriate modulation is applied to the NV spins such that $F_t(\omega)/(\omega^2 t) = \delta(\omega - \omega_0)$, i.e., if a Dirac δ -function is localized at a desired frequency ω_0 , then $\chi(t) = tS(\omega_0)/\pi$. Therefore, by measuring the time-dependence of the qubit coherence $C(t)$ when subjected to such a “spectral δ -function” modulation, we can extract the spin bath’s spectral component at frequency ω_0 :

$$S(\omega_0) = -\pi \ln(C(t))/t. \quad (2)$$

This procedure can then be repeated for different values of ω_0 to provide complete spectral decomposition of the spin environment.

A close approximation to the ideal spectral filter function $F_t(\omega)$ described above can be provided by a variation on the well-known CPMG pulse sequence for dynamical decoupling of a qubit from its environment [26] (Fig. 1(d)). The CPMG pulse sequence is an extension of the

Hahn-echo sequence [27] (Fig. 1(d)), with n equally-spaced π -pulses applied to the system after initially rotating it into the x-axis with a $\pi/2$ -pulse. We apply a deconvolution procedure to correct for deviations of this filter function from the ideal Dirac δ -function (see Supplement).

The composite solid-state spin environment in diamond is dominated by a bath of fluctuating N electronic spin impurities, which causes decoherence of the probed NV electron-spin qubits through magnetic dipolar interactions. In the regime of low external magnetic fields and room temperature (relevant to the present experiments), the N bath spins are randomly oriented, and their flip-flops (spin state exchanges) can be considered as random uncorrelated events [17]. Therefore, the resulting spectrum of the N bath's coupling to the NV spins can be assumed to be Lorentzian [24]:

$$S(\omega) = \frac{\Delta^2 \tau_c}{\pi} \frac{1}{1 + (\omega \tau_c)^2}. \quad (3)$$

This spin bath spectrum is characterized by two parameters: Δ is the average coupling strength of the N bath to the probed NV spins; and τ_c is the correlation time of the N bath spins with each other, which is related to their characteristic flip-flop time. In general, the coupling strength Δ is given by the average dipolar interaction energy between the bath spins and the NV spins, and the correlation time τ_c is given by the inverse of the dipolar interaction energy between neighboring bath-spins. Since such spin-spin interactions scale as $1/r^3$, where r is the distance between spins, it is expected that the coupling strength scales as the N bath spin density n_{spin} (i.e., $\Delta \propto n_{spin}$), and the correlation time scales as the inverse of this density (i.e., $\tau_c \propto 1/n_{spin}$).

Note also that the multi-pulse CPMG sequence used in this spectral decomposition technique extends the NV spin coherence lifetime by suppressing the time-averaged coupling to the fluctuating spin environment. In general, the coherence lifetime T_2 increases with the number of pulses n employed in the CPMG sequence. For a Lorentzian bath, in the limit of very short correlation times ($\tau_c \ll T_2$), the sequence is inefficient and $T_2 \propto n^0$ (no improvement with number of pulses). In the opposite limit of very long correlation times ($\tau_c \gg T_2$), the scaling is $T_2 \propto n^{2/3}$ [5, 28, 29] (see also recent work on quantum dots [30]).

Experimentally, we manipulate the $|0\rangle$ - $|1\rangle$ spin manifold of the NV triplet electronic ground-state using a static magnetic field and resonant microwave pulses; and employ a 532 nm laser to

TABLE I. Comparison of key characteristics and extracted “average-fit” Lorentzian spin bath parameters for the NV-diamond samples studied in this work.

	^{12}C	Apollo	HPHT
Meas. technique	wide-field	wide-field	confocal
N concentration	~ 1 ppm	~ 100 ppm	~ 50 ppm
NV density	$\sim 10^{14}[\text{cm}^{-3}]$	$\sim 10^{16}[\text{cm}^{-3}]$	$\sim 10^{12}[\text{cm}^{-3}]$
^{13}C concentration	0.01%	1.1%	1.1%
Echo (1-pulse) T_2	240(6) μs	2(1) μs	5(1) μs
T_2 scaling	$n^{0.43(6)}$	$n^{0.65(5)}$	$n^{0.7(1)}$
Max. achieved T_2	2.2 ms	20 μs	35 μs
Δ (expected)	≈ 60 kHz	≈ 6 MHz	≈ 3 MHz
Δ (measured)	30(10) kHz	7(3) MHz	1(1) MHz
τ_c (expected)	≈ 15 μs	≈ 0.17 μs	≈ 0.34 μs
τ_c (measured)	10(5) μs	3(2) μs	10(5) μs
FOM [ms/cm^3]	2×10^{14}	2×10^{14}	10^{10}

initialize and provide optical readout of the NV spin states (Fig. 1(c); for details see Supplement and [10, 13, 14]).

We applied the spectral decomposition technique to extract the spin bath parameters Δ and τ_c as well as the NV multi-qubit coherence FOM for three diamond samples with differing NV densities and concentrations of electronic and nuclear spin impurities (see Table I): (1) An isotopically pure ^{12}C diamond sample grown with chemical vapor deposition (CVD) techniques (Element 6), was studied using an NV wide-field microscope [13]. This sample has a very low concentration of ^{13}C nuclear spin impurities (0.01%), a moderate concentration of N electronic spin impurities (~ 1 ppm), and a moderate NV density ($\sim 10^{14}[\text{cm}^{-3}]$). (2) A thin-layer CVD diamond sample (Apollo) with natural ^{13}C concentration (1.1%), high N concentration (~ 100 ppm), and large NV density ($\sim 10^{16}[\text{cm}^{-3}]$) was also studied using the NV wide-field microscope. (3) A type 1b high-pressure high-temperature (HPHT) diamond sample (Element 6) with natural ^{13}C concentration, high N concentration (~ 50 ppm), and low NV density ($\sim 10^{12}[\text{cm}^{-3}]$) was studied using a confocal

apparatus able to measure single NV centers.

The results for the ^{12}C sample are summarized in Fig. 2. We find that the best-fit Lorentzian spin bath spectrum (fit to the average of all data points) has coupling strength of $\Delta = 30 \pm 10$ kHz and correlation time $\tau_c = 10 \pm 5 \mu\text{s}$, which agrees well with the range of values we find for the Lorentzian spin bath spectra $S_n(\omega)$ fit to each pulse sequence individually, $\Delta \simeq 30 - 50$ kHz, $\tau_c \simeq 5 - 15 \mu\text{s}$ (Fig. 2(a), see Supplement). These values are in reasonable agreement with the expected ‘‘N dominated bath’’ values for Δ and τ_c for this sample’s estimated concentrations of ^{13}C and N spins (see Table I). In Fig. 2(b) we plot the NV spin coherence lifetime T_2 , determined from the measured coherence decay $C_n(t)$, as a function of the number n of CPMG pulses.

The results of the spectral decomposition procedure for all three samples are summarized in Fig. 3 and Table I. There is reasonable agreement between the measured and expected values for the NV/spin-bath coupling strength Δ in all three NV-diamond samples, with Δ scaling approximately linearly with the N concentration. Similarly, the measured and expected values for the spin-bath correlation time τ_c agree well for the ^{12}C sample. However, we find a striking discrepancy between the measured and expected values of τ_c for the two samples with 1.1% ^{13}C concentration (Apollo and HPHT): both samples have measured spin bath correlation times that are more than an order of magnitude longer than given by the electronic spin bath model, though the relative values of τ_c for these two samples scale inversely with N concentration, as expected.

We explain this suppression of spin-bath dynamics as a result of random, relative detuning of electronic spin energy levels due to interactions between proximal electronic (N) and nuclear (^{13}C) spin impurities. The ensemble average effect of such random electronic-nuclear spin interactions is to induce an inhomogeneous broadening ΔE of the resonant electronic spin transitions in the bath, which reduces the electronic spin flip-flop rate R given by [31, 32]

$$R \simeq \frac{\pi}{9} \frac{\Delta_N^2}{\Delta E}, \quad (4)$$

where Δ_N is the dipolar interaction between N electronic spins. In this physical picture, ΔE is proportional to the concentration of ^{13}C impurities and to the N- ^{13}C hyperfine interaction energy; whereas Δ_N is proportional to the N concentration. Given the magnetic moments and concen-

trations of the N and ^{13}C spin impurities, and the large N- ^{13}C hyperfine interaction in diamond [33], we estimate $\Delta E \sim 10$ MHz and $\Delta_N \sim 1$ MHz for the Apollo and HPHT samples, which implies an order of magnitude suppression of R compared to the bare flip-flop rate ($R_{bare} \sim \Delta_N$), consistent with our experimental results (see Table I).

Importantly, we found large values for the multi-qubit FOM $\sim 2 \times 10^{14}[\text{ms}/\text{cm}^3]$ for both the ^{12}C and Apollo samples. (The HPHT sample has a relatively low FOM, as expected given its low NV density.) The long coherence time obtained for the Apollo sample, with high NV density and N concentration, is a result of the combined effect of suppression of electronic spin bath dynamics by nuclear spin impurities and dynamical decoupling: the extended spin bath correlation time enhances the effectiveness of dynamical decoupling, such that T_2 is increased by a factor of ~ 10 despite the large concentration of N impurities.

In summary, we applied a spectral decomposition technique to three NV-diamond samples with different composite-spin environments to characterize the spin-bath dynamics and determine the NV multi-spin-qubit Figure-of-Merit (FOM). For samples with a finite concentration of ^{13}C nuclear spin impurities, this technique revealed an order-of-magnitude suppression of the N electronic spin bath dynamics, which can be explained by random interactions between proximal electronic and nuclear spin impurities. This spin-bath suppression enhances the efficacy of dynamical decoupling for samples with high N impurity concentration, enabling increased NV spin coherence times and thus realization of a FOM $\sim 2 \times 10^{14}[\text{ms}/\text{cm}^3]$, which is larger than any other room temperature solid-state system and within an order of magnitude of the state-of-the-art spin coherence FOM achieved in atomic systems [15]. Further optimization of the multi-spin-qubit FOM may be possible by engineering this spin-bath suppression, e.g., with ^{13}C concentration higher than the natural value. The present results, together with the possibility of single qubit addressability through AFM [34–36] or super-resolution techniques [37] and intrinsic qubit-qubit interactions [1], pave the way for quantum information, sensing and metrology applications in a robust, scalable, multi-qubit solid-state architecture. Finally, the spectral decomposition technique presented here, based on well-known pulse sequences and a simple reconstruction algorithm, can be applied to other composite solid-state spin systems, such as quantum dots and phosphorous

donors in silicon. Such measurements could provide a powerful approach for the study of many-body dynamics of complex spin environments, potentially exhibiting similar effects related to the interplay between nuclear and electronic spin baths.

We gratefully acknowledge fruitful discussions with Patrick Maletinsky and Shimon Kolkowitz; and assistance with samples by Daniel Twitchen and Matthew Markham (Element 6) and Patrick Doering and Robert Linares (Apollo). This work was supported by NIST, NSF and DARPA (QuEST and QuASAR programs).

-
- [1] Jiang, L. *et al.* Repetitive readout of a single electronic spin via quantum logic with nuclear spin ancillae. *Science* **326**, 267–272 (2009).
 - [2] Neumann, P. *et al.* Single-shot readout of a single nuclear spin. *Science* **329**, 542–544 (2010).
 - [3] McCamey, D. R., Van Tol, J., Morley, G. W. & Boehme, C. Electronic spin storage in an electrically readable nuclear spin memory with a lifetime > 100 seconds. *Science* **330**, 1652–1656 (2010).
 - [4] Zurek, W. H. Decoherence, einselection, and the quantum origins of the classical. *Rev. Mod. Phys.* **75**, 715–775 (2003).
 - [5] Taylor, J. M. *et al.* High-sensitivity diamond magnetometer with nanoscale resolution. *Nat. Phys.* **4**, 810–816 (2008).
 - [6] Maze, J. R. *et al.* Nanoscale magnetic sensing with an individual electronic spin in diamond. *Nature* **455**, 644–647 (2008).
 - [7] Balasubramanian, G. *et al.* Nanoscale imaging magnetometry with diamond spins under ambient conditions. *Nature* **455**, 648–651 (2008).
 - [8] Goldstein, G. *et al.* Environment-assisted precision measurement. *Phys. Rev. Lett.* **106**, 140502 (2011).
 - [9] Acosta, V. M. *et al.* Diamonds with a high density of nitrogen-vacancy centers for magnetometry applications. *Phys. Rev. B* **80**, 115202 (2009).
 - [10] Childress, L. *et al.* Coherent dynamics of coupled electron and nuclear spin qubits in diamond. *Science* **314**, 281–285 (2006).
 - [11] Tyryshkin, A. M., Lyon, S. A., Astashkin, A. V. & Raitsimring, A. M. Electron spin relaxation times of phosphorus donors in silicon. *Phys. Rev. B* **68**, 193207 (2003).
 - [12] Hanson, R., Kouwenhoven, L. P., Petta, J. R., Tarucha, S. & Vandersypen, L. M. K. Spins in few-

- electron quantum dots. *Rev. Mod. Phys.* **79**, 1217–1265 (2007).
- [13] Pham, L. M. *et al.* Magnetic field imaging with nitrogen-vacancy ensembles. *New Journal of Physics* **13**, 045021 (2011).
- [14] Stanwix, P. L. *et al.* Coherence of nitrogen-vacancy electronic spin ensembles in diamond. *Phys. Rev. B* **82**, 201201 (2010).
- [15] Allred, J. C., Lyman, R. N., Kornack, T. W. & Romalis, M. V. High-sensitivity atomic magnetometer unaffected by spin-exchange relaxation. *Phys. Rev. Lett.* **89**, 130801 (2002).
- [16] Dobrovitski, V. V., Feiguin, A. E., Awschalom, D. D. & Hanson, R. Decoherence dynamics of a single spin versus spin ensemble. *Phys. Rev. B* **77**, 245212 (2008).
- [17] Barnes, E., Cywiński, Ł. & Das Sarma, S. Master equation approach to the central spin decoherence problem: the uniform coupling model and the role of projection operators. *ArXiv e-prints* (2011). 1108.1199.
- [18] de Lange, G., Wang, Z. H., Rist, D., Dobrovitski, V. V. & Hanson, R. Universal dynamical decoupling of a single solid-state spin from a spin bath. *Science* **330**, 60–63 (2010).
- [19] Ryan, C. A., Hodges, J. S. & Cory, D. G. Robust decoupling techniques to extend quantum coherence in diamond. *Phys. Rev. Lett.* **105**, 200402 (2010).
- [20] Almog, I. *et al.* Direct measurement of the system-environment coupling as a tool for understanding decoherence and dynamical decoupling. *Arxiv*: 1103.1104v1 (2011).
- [21] Bylander, J. *et al.* Noise spectroscopy through dynamical decoupling with a superconducting flux qubit. *Nature Physics* **7**, 565–570 (2011).
- [22] Álvarez, G. A. & Suter, D. Measuring the spectrum of colored noise by dynamical decoupling. *Phys. Rev. Lett.* **107**, 230501 (2011).
- [23] Du, J. *et al.* Preserving electron spin coherence in solids by optimal dynamical decoupling. *Nature* **461**, 1265–8 (2009).
- [24] Klauder, J. R. & Anderson, P. W. Spectral diffusion decay in spin resonance experiments. *Phys. Rev.* **125**, 912–932 (1962).
- [25] Gordon, G., Erez, N. & Kurizki, G. Universal dynamical decoherence control of noisy single- and multi-qubit systems. *J. Phys. B* **40**, S75 (2007).
- [26] Meiboom, S. & Gill, D. Modified spin-echo method for measuring nuclear relaxation times. *Review of Scientific Instruments* **29**, 688–691 (1958).
- [27] Hahn, E. L. Spin echoes. *Phys. Rev.* **80**, 580–594 (1950).

- [28] Slichter, C. P. *Principles of magnetic resonance* (Springer-Verlag, 1990).
- [29] de Lange, G., Ristè, D., Dobrovitski, V. V. & Hanson, R. Single-spin magnetometry with multipulse sensing sequences. *Phys. Rev. Lett.* **106**, 080802 (2011).
- [30] Medford, J. *et al.* Scaling of Dynamical Decoupling for Spin Qubits. *ArXiv e-prints* (2011). 1108.3682.
- [31] de Sousa, R. & Das Sarma, S. Electron spin coherence in semiconductors: Considerations for a spin-based solid-state quantum computer architecture. *Phys. Rev. B* **67**, 033301 (2003).
- [32] Witzel, W. M., Carroll, M. S., Morello, A., Cywiński, L. & Das Sarma, S. Electron spin decoherence in isotope-enriched silicon. *Phys. Rev. Lett.* **105**, 187602 (2010).
- [33] Barklie, R. C. & Guven, J. ^{13}C hyperfine structure and relaxation times of the p1 center in diamond. *J. Phys. C* **14**, 3621 (1981).
- [34] Grinolds, M. S. *et al.* Quantum control of proximal spins using nanoscale magnetic resonance imaging. *Nature Physics* **7**, 687–692 (2011).
- [35] Arcizet, O. *et al.* A single nitrogen-vacancy defect coupled to a nanomechanical oscillator. *Nature Physics* **7**, 879–883 (2011).
- [36] Maletinsky, P. *et al.* A robust, scanning quantum system for nanoscale sensing and imaging. *ArXiv e-prints* (2011). 1108.4437v1.
- [37] Maurer, P. C. *et al.* Far-field optical imaging and manipulation of individual spins with nanoscale resolution. *Nature Physics* **6**, 912–918 (2010).

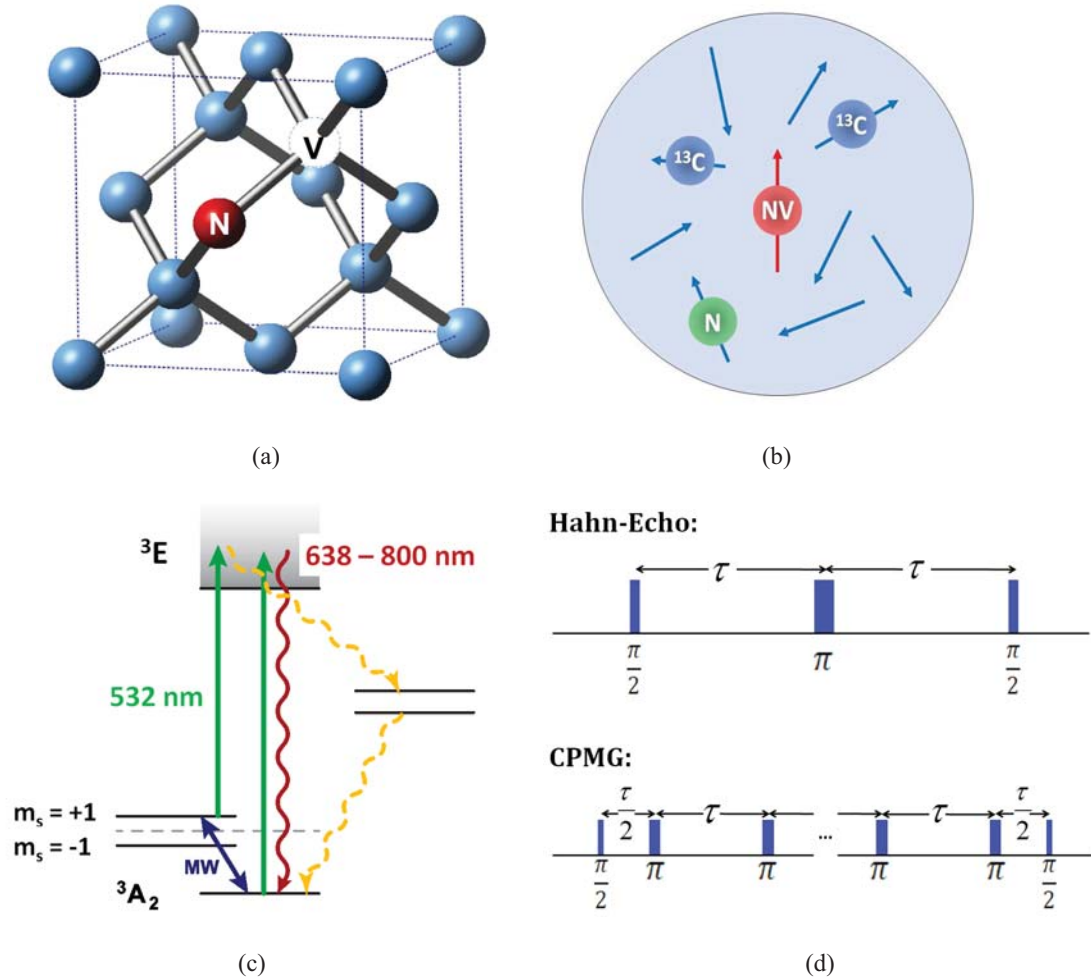
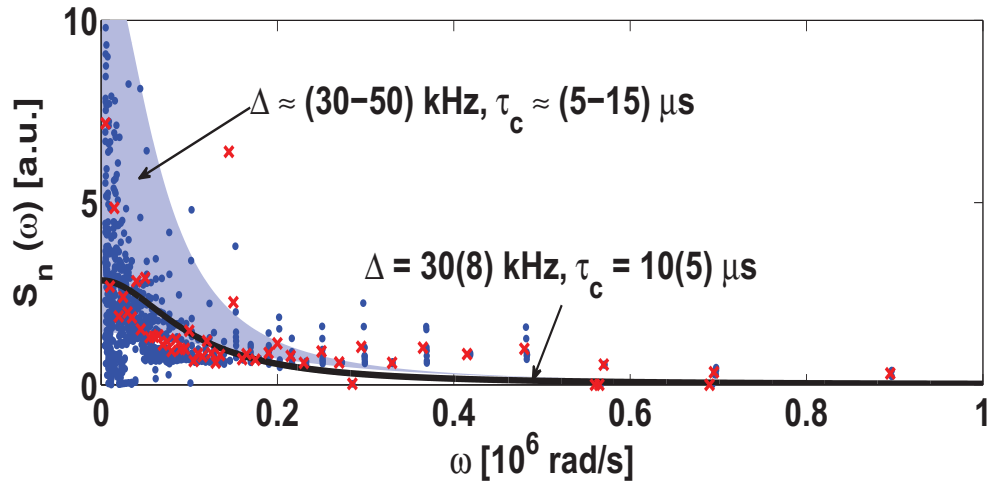
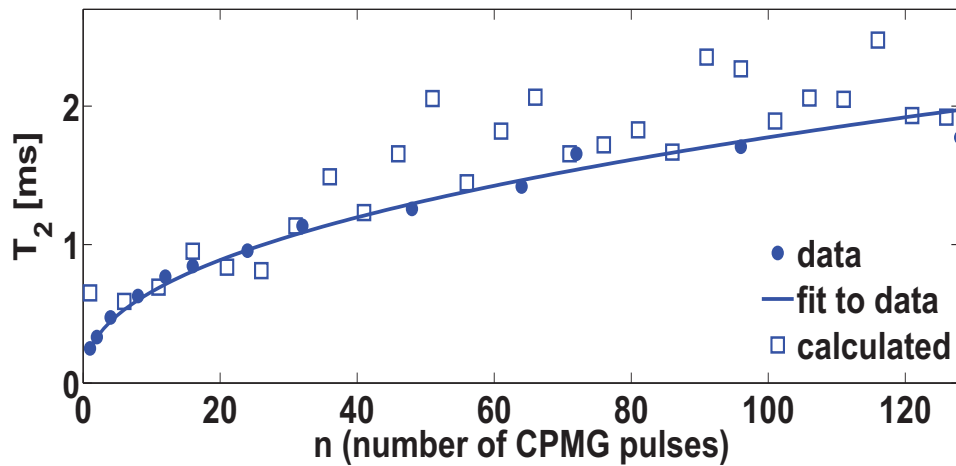


FIG. 1. Quantum spin in a solid-state environment (NV-center in diamond) and the applied spin-control pulse-sequences. (a) Lattice structure of diamond with a Nitrogen-Vacancy (NV) color center. (b) Magnetic environment of the NV center electronic spin: ^{13}C nuclear spin impurities and N electronic spin impurities. (c) Energy-level schematic of the NV center. (d) Hahn-echo and multi-pulse (CPMG) spin-control sequences.

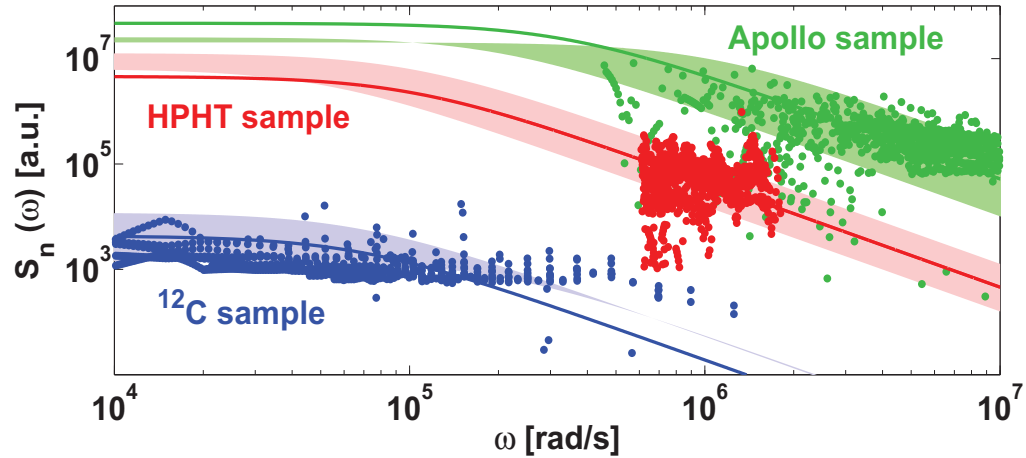


(a)

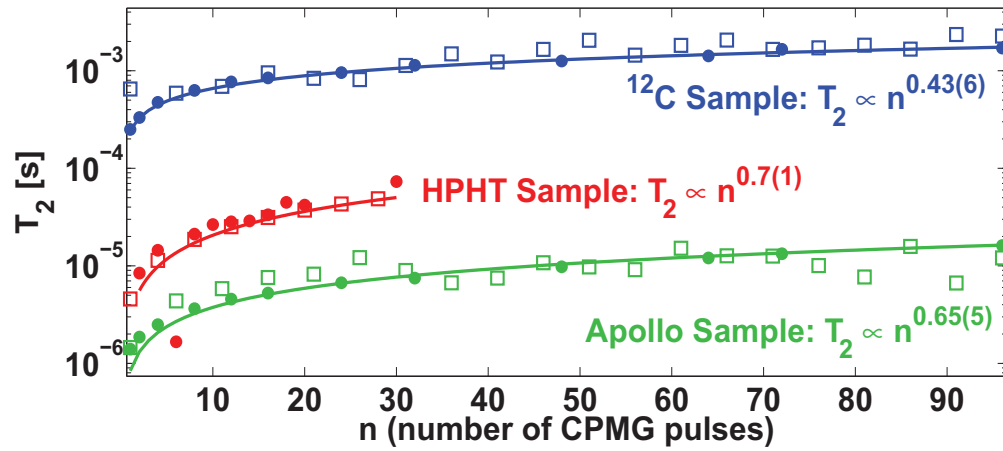


(b)

FIG. 2. Application of the spectral decomposition technique to an isotopically pure ^{12}C NV-diamond sample. (a) Derived values for the spin bath spectral functions $S_n(\omega)$ for all CPMG pulse sequences (blue dots) and average values at each frequency (red crosses); best fit Lorentzian for the mean spectral function $\langle S_n(\omega) \rangle_n$ (solid black line); and range of best-fit Lorentzians for the individual spectral functions $S_n(\omega)$ for each CPMG pulse sequence (grey band). (b) Scaling of T_2 with the number n of CPMG pulses: derived from NV spin coherence decay data $C_n(t)$ (dots); fit of dots to a power law $T_2 = 250(40)\mu\text{s} \times n^{0.43(6)}$ (solid line); and synthesized from the average-fit Lorentzian spin bath spectrum $\Delta = 30\text{ kHz}$, $\tau_c = 10\mu\text{s}$ (open squares), which yields a consistent fit $T_2 = 270(100)\mu\text{s} \times n^{0.4(1)}$.



(a)



(b)

FIG. 3. Comparative application of the spectral decomposition technique to the ^{12}C , Apollo and HPHT NV-diamond samples. (a) Spin bath spectral functions and associated Lorentzian fits using the average-fit method (solid lines) and the individual-fit method (color bands). (b) Scaling of T_2 with the number of CPMG pulses: dots - derived from NV spin coherence decay data $C_n(t)$; solid lines - fit of dots to a power law; open squares - synthesized from the average-fit Lorentzian spin bath spectrum.